The Nature of Cohesion Forces in Hardened Cement-based Materials: The View from the Nano-scale

R. J.-M. Pelleng [1], A. Gmira [2], H. Van damme [3]

[1] *Centre de Recherche en Matière Condensee et Nanosciences, CNRS, Campus de Luminy, 13288, Marseille cedex 09, France,* [2]*Department of Physics, Norwegian University of Science and Technology, NTNU, Trondheim, Norway,* [3]*Ecole Superieure de Physique et de Chimie Industrielles (ESPCI), 10 Rue Vauquelin, 75005 Paris, France.*
pelleng@crmcn.univ-mrs.fr

Abstract

We explore the possible reasons for the high cohesion of hardened cement-based materials in terms of inter-particle forces using a combination of atomistic numerical methods: *ab initio*, molecular dynamics and (free) energy minimization techniques. Considering hardened C-S-H (calcium silicate hydrates) as being made of randomly oriented bricks, each brick made of a piling of few tobermorite layers, we found strong arguments for predicting that intra brick attractive electrostatic forces are the essential components of the cohesion of C-S-H. This is a consequence of the iono-covalent character of in-layer chemical bonds and results in strongly localized interlayer calcium ions and water molecules. We also report reference values for elastic properties of Tobermorite-like models of C-S-H.

1. Introduction

It is now clear that any source of progress in understanding cement cohesion is to be found at the nanometric scale using physical chemistry concepts. In the present paper, we discuss the use a new route towards a fundamental understanding of mechanical performances of cement materials. It is based on the engineering of the bonding scheme in the cement hydrate phase (C-S-H) at molecular level. In this approach, C-S-H is undoubtedly the main target since it is the major source of cohesion in materials made from ordinary Portland cement. A possible strategy, which is expected to increase rigidity and strength while maintaining an essentially brittle behaviour, could be the optimization of the forces which are giving C-S-H its remarkable cohesion, in spite of its porous structure and in spite of the presence of water between the individual nano-particles. The prerequisite for this is to know quite accurately the nature of those surface forces and the chemical parameters that control them. The point in the present paper is to review our present knowledge of the cohesion forces in C-S-H based on molecular simulation and *ab initio* calculations.

2. The nanotexture of C-S-H

2.1. The C-S-H phase

Though generally poorly organized (hence the widespread use of the words “C-S-H gel”), C-S-H is widely recognized to have a layered crystal structure, akin to that of the mineral tobermorite, with a layer (or lamella) thickness in the nanometrer range [1,2] (see below). This morphology is hardly recognizable in real hardened cement paste but it is evident from X-ray diffraction and from direct transmission electron microscopy (TEM) observations of pouzzolanic C-S-H (Fig.1).

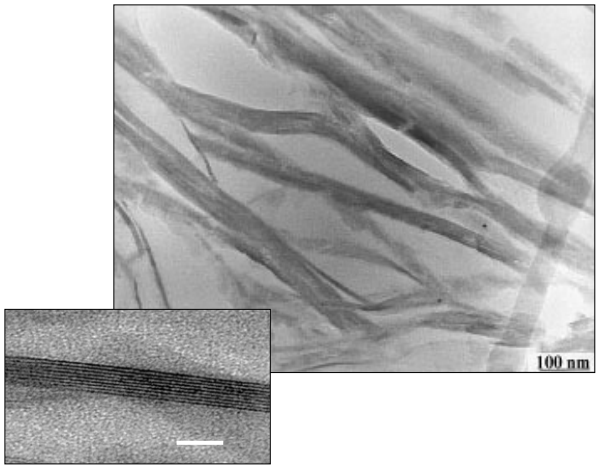

Figure 1. TEM micrographs of C-S-H with Ca/Si = 0.9, prepared by reaction of silica in a lime solution (scale bar in inset: 15 nm) [from ref 18].

The problem is to know how this highly anisotropic structure at the nanometer level evolves towards a basically isotropic material at larger length scales. C-S-H growth is not a simple process. Direct observation by AFM of the C-S-H nanoparticles grown on alite, silica or calcite surfaces at the solid-solution interface reveals the formation of well individualized and more or less elongated 5 nm thick disk-shaped particles with a long axis of the order of 60 nm [3,4]. Each particle or elementary brick is in fact an ordered aggregate of a few C-S-H lamellae, similar to those of the TEM micrograph of figure 1, but with a much less developed lateral extension. Further hydration leads to a multiplication of the C-S-H particles, leading to larger assemblies. These assemblies may grow either laterally, parallel to the substrate surface, or axially, perpendicular to the surface. Lateral growth is always faster, but the ratio of axial over lateral growth depends on the lime concentration in the solution, large lime concentrations favouring the axial growth of high Ca/Si C-S-H. The first layers of particles look remarkably well organized but, as the thickness of the layer increases, its roughness increases also and it tends to loose order. This is a very general phenomenon expected for many random growth processes on solid surfaces [5]. Such detailed observations cannot be performed on real dense pastes, but numerous models have been proposed on the basis of indirect data such as surface area and porosity determinations. A

recent one [6] assumes the existence of two types of aggregates, compact and loose. On the other hand, there is now a considerable body of evidence, from a variety of techniques [7] that, at high degrees of hydration, the texture exhibits scale invariant (fractal) properties from, at least, the nm to the µm scale. A key question is to know whether the basic nanostructure-forming unit in a dense paste is a single C-S-H layer or an ordered aggregate. This is not an innocent question because, in the first case, one may expect some entanglement between aggregates (the same elementary layer may be involved in two or more different aggregates), whereas, in the second case, the aggregates should be considered as structurally independent units interacting by surface forces. As far as we are aware, this is still an open question. A reasonable cartoon, inspired from the pioneering work of Powers [8] and from TEM micrographs [9], emphasizing continuity and entanglement, is shown in figure 2.

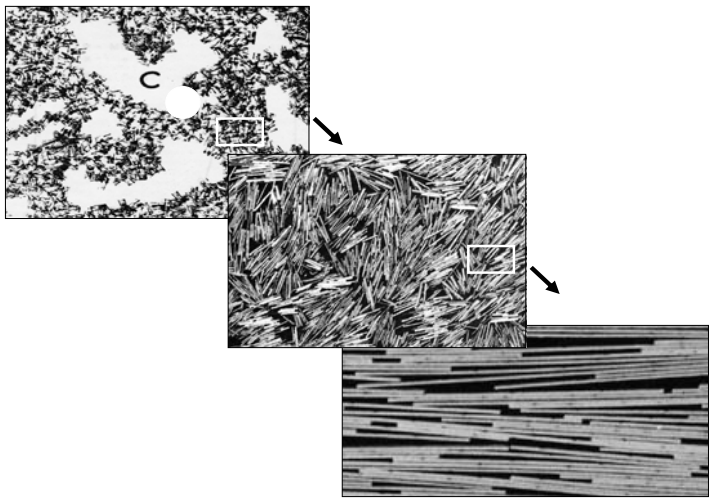

Figure 2. A cartoon inspired from the pioneering work of Powers, illustrating the hierarchy of local microstructures in dense C-S-H pastes. The important features are the locally ordered stacks of individual layers, defect regions of all sizes and entanglement.

What are the key microstructural features that should be retained from the previous discussion in order to build a realistic bonding scheme for a dense C-S-H hardened paste? Two features seem to be critical. The first is the existence of domains where the distance between individual C-S-H nanolayers (the interlamellar gap) is of the order of a few tenths of nm, i.e. of the same order as the interlayer distance in a tobermorite crystal with a 1.1 or 1.4 nm repeat distance for instance (see below). This would happen within the locally ordered aggregates and also at the contact or entanglement spots between stacks. The calcium ions in these very confined spaces may be expected to be strongly interacting with the negative surface groups of the silica chains of the C-S-H layers. The second important features are the domains (defect regions) where the distance between C-S-H layers is larger with, most probably a broad distribution. The calcium ions in those regions should be fully hydrated and highly mobile.

2.2. Tobermorite: a model for C-S-H at the nanoscale

We now turn to the structure of the C-S-H phase at an atomistic level. Several characterization techniques including solid state NMR [10,11,12,13], infra-red [14] and EXASF [15], have demonstrated its similarity with a layered mineral known as tobermorite. Tobermorite was firstly described by Heddle [16] in Tobermory (Scotland). Tobermorite polytypes may be classified on the basis of their basal spacing, which are related to their degrees of water content (defined here as degree of hydration, not tobe confused with the hydration of anhydrous C_3-S in the cement chemical reaction that produces C-S-H. Riversideite, more commonly called 9 Å tobermorite, has the chemical formula $Ca_5Si_6O_{16}(OH)_2$; 11 Å tobermorite is more hydrated, with a chemical composition ranging from $Ca_5Si_6O_{17}.5(OH)_2$ to $Ca_5Si_6O_{16}(OH)_2.5H_2O$; and finally 14 Å tobermorite, also known as plombierite, is the most hydrated phase of the group, with the chemical formula $Ca_5Si_6O_{16}(OH)_2.8H_2O$. These three different phases are characterized by basal spacing of 9.3, 11.3 and 14 Å, respectively [17]. Most researchers in cement chemistry identify poorly crystalline or amorphous C-S-H to 14 Å tobermorite.

14 Å tobermorite transforms to 11 Å tobermorite by heating from 60ºC to 100ºC; subsequent heating at 300ºC for few hours gives rise to 9 Å tobermorite. It was recently discovered that skrinking from the 14 to the 11 Å polytype was not reversible [18] by contrast to what usually assumed in standard text books on cement chemistry. Some specimens of 11 Å tobermorite do not shrink on dehydration and are called "anomalous Tobermorite" to distinguish them from those that shrink on dehydration called "normal tobermorite" [19]. The anomalous behavior upon dehydration is though to be the consequence of a significant amount of aluminum substituting silicon atoms in silicate chains and creating layer to layer bridges. In normal tobermorite, the Ca/Si ratio can vary from 0.83 (the value for 14 Å tobermorite) to about 1.5. Two atomistically resolved structures of tobermorite 11 Å are now available in the literature, one due to Hamid [20] and a second, more recent, due to Merlino *et al* [21]. Both are based on a composite layer of distorted central Ca-O sheet that is ribbed on either side with infinite dreierketten, *i.e.* silicate chains that repeat at an interval of three silicate tetrahedra. Two adjacent tetrahedra forming a so-called dimers coordinate through oxygens to in-layer calcium ions, while the third, called bridging tetrahedron, links two successive dimers. The interlayer space contains water molecules and additional calcium cations which amount directly depends on the number of layer OH groups that in turn depends on pH. In Hamid's model, the layers are not chemically bonded to each other and are electrically charged for Ca/Si ratio larger than 0.66. The main difference introduced in Merlino's model compared to the independent layer model of Hamid consists in the presence of Wollastonite chains (linked silicates tetrahedra between faced silicates chains) in 11 Å tobermorite without consideration of the normal or anomalous state. These layer to layer cross-over chemical linkages

induce the creation of cavities similar to those present in zeolitic materials. Discriminating between the two available tobermorite models is indeed one goal of the present study although the thermal transformation from 14 to 11 Å is rather consistent with texture made of independent layers; the 3 Å variation of the interlayer spacing being not compatible with chemical bonding. In a series of papers [22,23,24], we showed using a meso-scale simulation approach with a continuum description of solvent effects that during setting *i.e.* in a fully water saturated state, calcium density fluctuations close to tobermoritic charged surfaces are correlated and induce layer to layer attractive forces so-called ionic correlation forces [25]. This is though to describe interactions between C-S-H grains in defective regions with larger interlayer spacing.
In the present work, we focus on layer to layer cohesion in the partially hydrated conditions that occur at interdistance of about one nanometer or less (*i.e.* inside a pile of tobermoritic layers forming a C-S-H nanoparticle or at contact between of these nano objects). We wish to analyze the cohesion forces which may be acting in these environments. As discussed elsewhere, van der Waals and capillary forces contribute probably only marginally to the cohesion of hardened cement [26]. We will therefore concentrate on the forces generated by the presence of charged ions in very confined sub-nm regions using for the first time to our knowledge, a fully atomistic description.

3. Numerical methods

Atomistic computer simulation is now intensively used to understand properties and predict minerals behavior. Assuming as a starting point that C-S-H nanotexture can be described with the crystalline structure of tobermorite, time has come to use the various available numerical approaches (quantum and classical) in the field of cement physical chemistry.

3.1. From energy minimization to thermodynamics and elastic properties using empirical interatomic potentials

At a first step, we used a (0K) energy minimization technique with the GULP code [27,28,29]. These calculations were performed using a set of empirical but transferable interatomic potentials calibrated on quartz and CaO compounds. Anions (here oxygens in tobermorite layers and in water molecules) were modeled as polarizable species using the core-shell model. These transferable empirical inter-atomic potentials based on the use of the formal electric charge for each interacting species, have reproduced successfully the structure and properties of many oxides [30] including silicates [31,32,33] and phyllosilicates [34,35] (see reference [36] for liquid water). They include two-body and three-body analytical functions that allow calculating the energy between pairs and triplets of atoms. They depend on the choice of some parameters that can be advantageously calibrated using *ab-initio* calculations in same simple cases; the transferability of such potential parameters in the case of more

complex systems can be then checked or assumed as in this work for the {Ca, Si, O, OH, H_2O} system. Note that the calculation of electrostatic interactions between pairs of ions is done with the Ewald summation scheme. The advantage of such an approach compared to *ab-initio* quantum mechanical methods is that one can compute for large systems with low symmetry, not only structural but also thermodynamic and elastic properties (from the elastic tensor using both Voigt and Reuss equations for bulk, shear and Young modulus). Reference [37] gives all details on such calculations in the case of Lizardite, a magnesium silicate.
Energy minimization for finding an equilibrium structure consists in tracking stationary points that correspond to a minimum energy gradient with positive energy curvature (*i.e.* finding a set of atomic positions that minimizes system energy and give a Hessian operator with positive eigenvalues only). A phonon spectrum calculation at the center of the Brillouin zone can be used as a final validation from which one gets the list of lattice vibration frequencies that should be all positive except the three first that should be zero (unit cell translational invariance). Such minimization procedure gives a zero temperature solution. If one aims at calculating system equilibrium properties at finite temperature then free energy calculations are to be considered. Along with Monte-Carlo or Molecular Dynamics simulations, a third possible route to study crystalline structures at a microscopic scale is thus the lattice dynamic theory. From the set of system Hessian eigenvalues, one can compute the vibration partition function in the harmonic approximation and deduce all thermodynamic functions including entropy hence system free energy. Energy minimizations are performed using the Newton-Raphson method. All degree of freedom were considered: atomic positions, unit cell dimensions and angles.

3.2. Periodic ab-initio calculations

At a second step, we used the fully GULP-relaxed structures as inputs for *ab initio* calculations using the CRYSTAL98 code for periodic systems. It allows calculating cohesion energy and obtaining a complete characterization of bonding processes in crystalline materials. The *ab-initio* method is based on the resolution of the Schrödinger equation using the Hartree-Fock approximation neglecting electron fluctuations hence correlations [38]. In this type of approach, all chemical elements in tobermorite unit cell are described using sets of atomic orbitals. Note that in the case of silicon and calcium, we used Barthelat pseudo-potentials for core electrons. For hydrogen and oxygen, all electrons are considered (STO3G and 4-11G atomic basis sets respectively) [39].

3.3. Molecular Dynamics simulations of interlayer Ca ions and H $_2$0

Using the same sets of empirical interatomic potentials as in the energy minimization step, we performed a molecular dynamics study using the Nosé-Hoover thermostat. We selected the optimized structures obtained by the energy minimisation procedure as starting configurations. The minimized cell dimensions and angles and slab species were kept fixed during the Molecular Dynamics (MD) runs and we followed the trajectories of interlayer calcium and water species. The MD simulations were performed at 310 K for 0.1 ns with a time step of 0.5 fs and a shell mass of 10 % of the total mass of oxygen ions. The trajectories were recorded every 0.005 ps. The Mean Square Displacements (MSD) for each interlayer species were then evaluated hence the self-diffusion coefficient using the Einstein equation. The internal energy at finite temperature was calculated as the canonical ensemble average of the potential energy while system pressure was calculated using the virial equation that requires calculating interatomic distances and resulting forces on each relaxing sites.

4. Results and discussion

Tables 1, 2 and 3 present (0K) energy minimization results for 11 Å tobermorite as described by Hamid and Merlino models respectively with Ca/Si ratio of 0.83 and unity and $4H_2O$/unit cell.

	a(Å)	b(Å)	c(Å)	α(°)	β(°)	γ(°)	CaO (Å)	SiO (Å)	O – Si – O (°)
Exp.	7.39	22.78	6.69	90.00	123.49	90.00	2.35-2.75	1.55-1.67	----
Sim.	7.30	24.50	6.65	90.28	123.75	89.93	2.35-2.67	1.49-1.67	100.61-119.35

Table 1. Energy minimization results for 11 Å tobermorite in Hamid's model (Ca/Si = 1.0, $4H_2O$/unit cell).

	a (Å)	b (Å)	c(Å)	α(°)	β(°)	γ(°)
Exp.	7.39	22.78	6.69	90.00	123.49	90.00
Sim.	7.38	23.26	6.75	90.00	123.28	90.00

Table 2. Energy minimization results for 11 Å tobermorite in Hamid's model (Ca/Si = 0.83, $4H_2O$/unit cell).

	a(Å)	b(Å)	c(Å)	α(°)	β(°)	γ(°)	CaO (Å)	SiO (Å)	O – Si – O (°)
Exp.	11.92	11.92	6.732	80.26	99.73	35.99	2.28-2.61	1.60-1.68	----
Sim.	12.61	11.75	6.713	98.61	107.2	35.66	2.22-2.43	1.54-1.66	98.81-124.2

Table 3. Energy minimization results for 11 Å Tobermorite in Merlino's model (Ca/Si = 0.83, $4H_2O$/unit cell).

As far structure information are concerned, we found that a better agreement between simulation and experiment with Hamid's model than with Merlino's. This can particularly noticeable when one looks at unit cell angles: the difference between experimental and simulated unit cell parameters is less than 3% for the structure proposed by Hamid and 12% for the characteristic angles in Merlino's structure. It seems that the set of interatomic potentials used here gives a fairly well description of Hamid's model of tobermorite (especially that with Ca/Si=0.83). In order to compare Hamid and Merlino models from an energy point of view, we chose to compare them using a density value criterion that is the unit cell energy after relaxation divided by its volume since it varies significantly from one model to the other. The density of energy calculated at the minimum of its energy *versus* the interlayer separation curve for Hamid's structure (with Ca/Si=1, table 1) is -2.07 eV/Å^3 while we find -2.15 eV/Å^3 for Merlino's model. Merlino's structure thus appears to be a few % more stable than that proposed by Hamid. This difference is not significant taking into account the flatness of the potential energy curve in the region of its minimum minimorum (fig 3): on this interlayer separation domain 11-13 Å, the energy density in Hamid's description, varies from -2.30 to -1.94 eV/Å^3. As demonstrated below, intra-layers bonds possess a large covalent character giving rise to partial electric charges that are smaller (in absolute value) than the formal ones. We confronted this result to its *ab initio* counter part. We then found that Hamid's structure is 8% more stable than Merlino's description (-0.41 eV/Å^3 and -0.380 eV/Å^3 respectively) although the latest consists in a 3D chemically bonded structure. The reasons for such a result has to be found is the larger (distance and angle) constrains in Merlino's model as compared to Hamid's. Of course, only the comparison of numbers obtained by a given approach is meaningful. In Figure 3, we present the variation of system potential energy as a function of the interlayer distance in the case of a hydrated ($4H_2O$/unit cell, Ca/Si=0.83) independent layer model of Tobermorite (Hamid's description) keeping all other unit cell parameters constant.

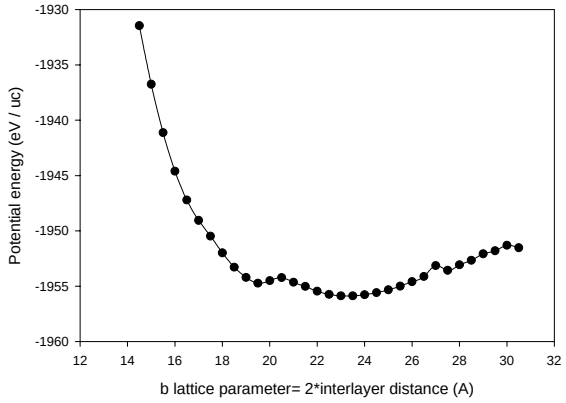

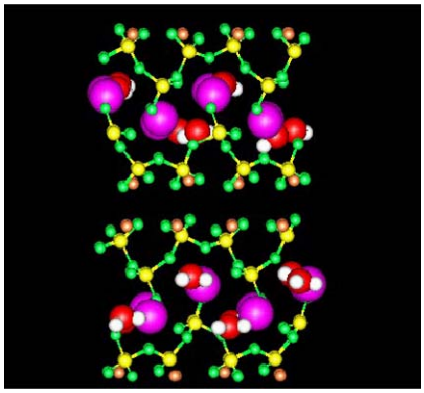

Figure 3. System potential energy as a function of the interlayer distance and a snapshot of the simulated system.

Ca/Si=1. It is interesting to notice the presence in such a potential energy curve at 0 K of three minima at 11, 12.25 and 14 Å, the later being less stable than the formers, in good agreement with the experimental results related below [18].The free energy at 300 K (not shown) have the same behavior as at 0 K, the gap between this two curves remains constant at large distance but varied slightly at short distance due to the vibrational entropy effect in this range.

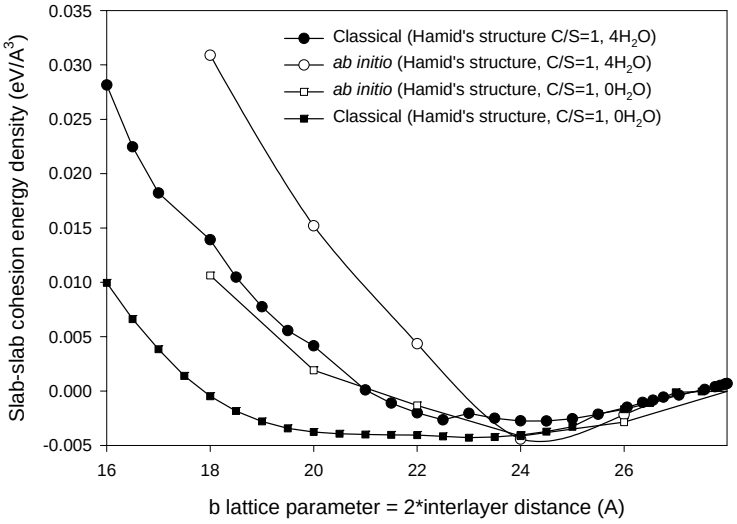

Figure 4: Comparison between classical and ab initio results for Tobermorite C/S=1 and two water content.

Figure 4 is a comparison between GULP and ab-initio calculations for the same Hamid's configuration (C/S=1, $4H_2O$/unit cell) taking the energy density at large interlayer distance as a reference. One notices that the slope of the repulsive inflection is more pronounced in the quantum approach than with the classical energy minimization method. For the same Tobermorite configuration, the dehydration enlarges the free energy well. Thus, the 11 Å-Tobermorite conformation is the more probable (more stable). Table 4 presents *ab initio* Mulliken electronic charges. One can see that these are smaller in absolute value than the formal charges. The ratio between Mulliken and formal charges quantifies the covalent character of the bonding process. In the case of tobermorite, we found that the iono-covalent character in around 60 %. This is not surprising for a (calcio) silicate. More interesting is the charge of the interlayer calcium that is also a fraction of the formal value indicating that there is some charge transfer between these species and the layers. This is the signature the existence of chemical bonds. This implies theses interlayer calcium ions are strongly bonded to the layers hence strongly localized. This is the reason for the non-exchangeable character of these ions on the contrary of the labile character of the interlayer ions in the clays for example. This further demonstrates that the primitive model (colloïdal approach) to tobermorite cohesion (based on the so-called ionic correlation attractive forces) that relies on fluctuations of interlayer calcium

density is not valid in the context of intra C-S-H crystallite cohesion [22,23,24] but retains some interesting features in the water saturated case that may be found at cement setting at early age and in larger inter-C-S-H crystallites voids.

	Si	Ca_{Layer}	Ca_{Inter}	O_{Layer}	O_{Water}	H_{Water}
q(ē)	+2.39 (+4)	+1.29 (+2)	+1.38 (+2)	-1.23 (-2)	-0.42 (-2)	+0.21 (+1)

Table 4: *ab initio* Mulliken charges in Hamid's model

It is also interesting to note that the Mulliken charges do not change when varying the interlayer distance from 7.5 to 16 Å. Varying the interlayer distance in Hamid's model does not change the nature of (interlayer) bonding that is therefore essentially electrostatic. The interlayer calcium species acts as water traps in the interlayer voids. The water molecules in their vicinity do not diffuse as revealed by their diffusion coefficient obtained from canonical molecular dynamics. We found that the diffusion coefficient of water molecules in the Tobermorite (C/S=1, $4H_20$/unit cell) interlayer space is nearly 1000 times smaller than that of liquid water. This confirms that interlayer species are very localized in rather well defined crystallographic sites. This is somewhat experimentally confirmed for other hydrated layered materials. Elastic properties of Tobermorite can be estimated for the relaxed configurations. Table 5 presents reference data for the set of inter-atomic potentials considered in this work following two

Voigt bulk modulus in GPa	35.4
Reuss bulk modulus in GPa	20.7
Voigt shear modulus in GPa	5.08
Reuss shear modulus in GPa	2.78
Voigt Poisson ratio	0.25
Reuss Poisson ratio	0.26
Young modulus along the x-z plane in GPa	94-91
Young modulus along the y (interlayer) direction in GPa	5
Average Young modulus in GPa	63.5

Table 5. Elastic properties of 14Å Tobermorite (C/S=0.83, $4H_20$/unit cell)

Voigt and Reuss routes (based on the elastic and compliance matrices respectively [37]). The simulated values of (average) young modulus and Poisson ratio compare rather well with mesoporosity-corrected experimental values obtained by nano-indentations [40,41].

5. Conclusion

In this study, we reported the ability of ionic (core-shell) empirical potentials in describing the stability and structural and elastic properties of Tobermorite taken as a model ot cement hydrate (CSH) at the sub-nanoscale as indicating by a large sets of experimental evidences; the texture of CSH at larger length scale as being a granular or a continuous medium is beyond the scope of the present work. Calculations performed by energy minimization and *ab initio* proved the Hamid's structure for tobermorite (independent layers) to be more stable than Merlino's model (linked layers). We further found that among the three energy minima at 9, 12.25 and 14 Å characteristics of the three known Tobermorite isomorphs, the most stable is the form that has an interlayer distance around 12 Å in agreement with experimental data. Analysis of *ab initio* Mulliken electric charges indicates a significant covalent character of the intra-layer bounds. We found that interlayer calcium ions are chemically bonded to the layers hence strongly localized. This is further confirmed when calculating the diffusion coefficient of confined water molecules attached to them that is found to be thousand times smaller than in the bulk liquid at room temperature. Finally we report elastic properties of tobermorite.

References

[1] H.F.W.Taylor, "Cement Chemistry", 2nd Edn., T. Telford Pub., London (1997).
[2] I. G. Richardson, Cem. Concr. Res., **29** (1999) 1131-1147.
[3] S. Gauffinet, E. Finot, A. Nonat, A. in "Hydration and Setting", A. Nonat, Ed., RILEM Publications S.A.R.L., Cachan (2000), 199-214.
[4] S. Gauffinet, E. Finot, E. Lesniewska, A. Nonat, C.R. Acad. Sci. Paris, Earth & Planetary Sciences, **327** (1998) 231-236.
[5] A.L. Barabassi, H. E. Stanley in "Fractal Concepts in Surface Growth", Cambridge University Press, Cambridge (1995), p 366.
[6] H.M. Jenning, Cem. Concr. Res., **30** (2000), 101-116.
[7] H. Van Damme in "Encyclopedia of Surface and Colloid Science", Marcel Dekker, Inc., New York, (2002) 1087-1103, and references therein.
[8] T. C. Powers, J. Am. Ceram. Soc., **41,** (1958) 1-6.
[9] R. Maggion, S. Bonnamy, P. Levitz, and H. Van Damme, H., in "The Modeling of Microstructure and its Potential for Studying Transport Properties and Durability", H. Jennings, J. Kropp, and K. Scrivener editors, *NATO ASI Series E : Applied Sciences* **304**, Kluwer Academic Publishers, Dordrecht (1996), 137-155.
[10] X. Cong, R. J. Kirkpatrick, J. Adv. Cem. Bas. Mat., **3** (1996), 144-156.
[11] X. Cong, R. J. Kirkpatrick, J. Am. Ceram. Soc., **79** (1996), 1585-1592.
[12] W. Wieker, A. R. Grimmer, A. Winkler, Cem. Concr. Res., **12** (1982), 333-339.
[13] S. Komarneni, D.M. Roy et al, Cem. Concr. Res. **17** (1987), 191-213.

[14] P. Yu, R. J. Kirkpatrick, B. Poe, P. F. McMillan, X. Cong, J. Am. Ceram. Soc., **82** (1999), 742-748.
[15] N. Lequeux, A. Moreau, S. Philippot, J. Am. Ceram. Soc., **8** (1999), 1299-1306.
[16] M. F. Heddle, Mineral. Mag., **4** (1880), 119-123.
[17] J. D. C. McConnell, Mineral.Mag., **30** (1954), 293-305.
[18] A. Gmira, PhD Thesis, University of Orléans, France (2003).
[19] T. Mitsuda and H. F. W. Taylor, Mineral. Mag., **42** (1978), 411-429.
[20] S. A Hamid, Zeitsch. Kristall., **154** (1981), 189-198.
[21] S. Merlino, E. Bonaccorsi and T. Armbruster, Amer. Mineral., 84 (1999), 1613-1621.
[22] R.J.-M. Pellenq, A. Delville, and H. Van Damme, in “Characterization of Porous Solids IV”, McEnaney, B., Mays et al ed., The Roy. Soc. Chem. Pub., Cambridge, 1997, 596-603.
[23] R. J.-M. Pellenq, J.-M. Caillol and A. Delville, J. Phys. Chem., **101** (1997) 8584-8594.
[24] A. Delville and R.J-.M. Pellenq, Mol. Sim., **24** (2000) 1-24.
[25] R. Kjellander, S. Marcelja, and J. P. Quirk, J. Coll. Interf. Sci., **126** (1988) 194-211.
[26] R. J.-M. Pellenq, H. van Damme, MRS Bulletin, 2004, 319-323.
[27] J. D. Gale, Phil. Mag. B, **73** (1996) 3-19.
[28] J. D. Gale, J. Chem. Soc. Faraday Trans., **93** (1997) 629-637.
[29] J. D. Gale, A. L. Rohl, Mol. Sim., **29** (2003) 291-341.
[30] N. H. de Leeuw, J. W. Watson, S. C. Parker, J. Phys. Chem., **99** (1995) 17219-17225.
[31] M. T. Dove, T. Cool, D. C. Palmer, A. Putnis, E. K. H. Salje and B. Winkler, Am. Mineral. **78** (1993) 486-492.
[32] G. D. Price, S. C. Parker, In Proceedings of NATO ASI on the physical properties and thermodynamic behavior of minerals, Ed. EKH Salje, Series C, **225** (1988) 591-618.
[33] B. Winkler, M. T. Dove, M. Leslie, Am. Mineral., **76** (1991) 313-331.
[34] D. R. Collins, C. R. A. Catlow, Am. Mineral., **77** (1992) 1172-1181.
[35] C. I. Saint-Diaz, A. Laguna-Hernandez, M. T. Dove, Phys. Chem. Min., **28** (2001) 130-141.
[36] N. H. De Leeuw, S. C. Parker, Phys. Rev. B., **58** (1998) 13901-13908.
[37] A-L. Auzende, R. J-M. Pellenq, B. Devouard, A. Baronnet, O. Grauby, Phys. Chem. Min., **33** (2006) 266-275.
[38] C. Pisani, "Lecture in chemistry", Quantum mechanical ab-initio calculation of the properties of crystalline materials, Ed. Springer 177 (1996).
[39] P. D’arco, M. Causa, C. Roetti, B. Silvi, Phys. Rev. B., **47** (1993) 3522-3529.
[40] J. Sanahuja, L. Dormieu, Ecole Nationale des Ponts et Chaussées, Paris, private communication
[41] F. J. Ulm, MIT, private communication